Modeling of Rebound Phenomenon of a Rigid Ball with Friction and Elastic Effects

Akira Nakashima, Yuki Ogawa, Yosuke Kobayashi and Yoshikazu Hayakawa

***Abstract*— We derive analytical models of the rebound phenomenon between a ping-pong ball and the table/racket rubber. In the rebound model of the table, the determination of the type of the contact during the impact is derived as a generalized condition in the 3-dimensional space. In the model between the ball and racket rubber, it is assumed that the kinetic energy of the tangent velocity is stored as the potential energy due to the elasticity of the rubber. This assumption leads to that the impulse in the horizontal direction is proportional to the tangent velocity. The models are verified by experimental data.**

I. Introduction

It is a challenging task for a robot to play table tennis with a human because playing table tennis is a dexterous task for humans. For simplicity, consider the situation of Fig. 1, where a robot tries to hit a flying ball. The dexterous can be implied by the strategy of the robot playing table tennis, which can be decomposed as the following subtasks: 1) To detect the states of the flying ball with vision sensors; 2) To predict the ball trajectory; 3) To determine the trajectory of the racket attached to the robot for hitting the ball to achieve desired trajectory. The number 1) means the image processing algorithm to obtain the position, the translational and rotational velocities of the ball. The number 2) means the prediction of the position and translational/rotational velocities of the ball for the next task of the determination. The number 3) means the determination of the trajectories of the position and orientation of the racket attached to the robot for the ball to follow desired trajectory. In the subtasks 2) and 3), the ball *rebounds* from the table and the racket rubber. It is therefore necessary to model the rebound phenomenon between the ball and the table/rubber in order to achieve the subtasks 2) and 3).

Fig. 1. A robot tries to hit a flying ball.

Authors are with Mechanical Science and Engineering, Graduate School of Engineering, Nagoya University, Furo-cho, Chikusa-ku, Nagoya, Japan akira@haya.nuem.nagoya-u.ac.jp, and Y. Hayakawa is also with RIKEN-TRI Collaboration Center, RIKEN, 2271-103, Anagahora, Shimoshidami, Moriyama-ku, Nagoya, Japan.

The rebound phenomenon between a ball and a surface has been studied by many researchers. Garwin [1] proposed the coefficient of restitution (COR) in the direction *parallel* to the surface. He determined from experimental data which the contact is the rolling, sliding or both together during the impact and whether the kinetic energy is stored as *elastic* one or not. Brody [2] considered the effect of *friction* of the surface with the assumption of no compression of the ball. He derived the condition of the rolling contact which is related to the translational and rotational velocities just before the rebound. Shibukawa [3] derived the condition which determines whether the rolling contact happens or not during the impact. As specified situations of the rebound, Cross [4] considered the effect of friction between the ball and strings of a racket in tennis. He also considered other situations, e.g., the horizontal COR between balls of various properties and a solid surface [5]. Furthermore, he investigated the bounce of a spinning ball being incident near the normal to the surface as an example of situations of hitting a ball by a racket [6]. For the normal COR, Cross [7] investigated the relation between the normal COR and the dynamics hysteresis of the impact force.

From the reviewed studies, the friction and elastic effects are very important facts in the rebound phenomenon. It is here assumed that a table tennis ball does not deform when rebounding. The friction effect is dominative in the case of the rebound on the table and determines the type of the contact (sliding/rolling) during the impact, while the elastic effect is dominative in the case of the rebound on the racket. As mentioned in the above reviews, these effects are not considered analytically in the rebound. The friction effect was considered in only the 2-dimensional case in [3] and the elastic effect was considered only experimentally in the some previous mentioned studies.

We derive analytical models of the rebound phenomenon between a ping-pong ball and the table/racket rubber. In the rebound model of the table, the determination of the type of the contact during the impact is derived as a generalized condition in the 3-dimensional space. In the model between the ball and racket rubber, it is assumed that the kinetic energy of the tangent velocity is stored as the potential energy due to the elasticity of the rubber. This assumption leads to that the impulse in the horizontal direction is proportional to the tangent velocity. The models are verified by experimental data.

II. Experimental System and Ball Detection

Fig. 2 shows the experimental system for detecting the

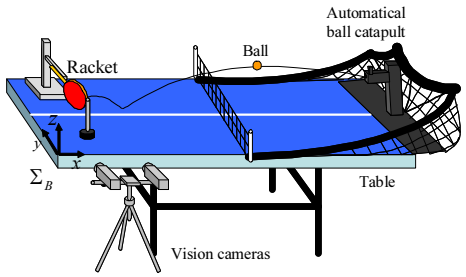

Fig. 2. Experimental system.

ball states. The table is an international standard one with the size of 1525(W)×760(H)×2740(D) [mm]. The ball is shot out from the automatical ball catapult ROBO-PONG 2040 (SAN-EI Co.) which is set at the end of the table. The flying ball is measured by the high-speed vision sensors with 900 [fps] (Hamamatsu Photonics K.K.). The array and pixel sizes per meter are 232×232 and $\alpha_u, \alpha_v = 2.0 \times 10^{-5}$ [pixel/m]. The sampled data are quantized as 2D image data with the monochrome brightness of 8bit (0–255). The focal length of the lens is $f = 35$ [mm] and the chip size is 13.0×14.3 [mm]. Σ_B is the reference frame. The racket is a standard one (Butterfly K.K.) which is fixed with respect to Σ_B and is mounted such that its contact surface is normal to the x-axis. The cameras are calibrated with respect to Σ_B.

The translational and rotational velocities are calculated as the constant by assuming that there is no effect of the air resistance. Figure 3 shows an example of the image processing. The figure (a) is the image data where the there are the racket and the ball with the black feature points. The figure (b) is the binarized one with an appropriate threshold. The white circle represents the ball. In the figure (c), the green closed line is the boundary of the ball. The four yellow points on the boundary of the ball are detected by the simple scannings as in the figures (c-1)–(c-4). In the scanning of (c-1), the arrows are scanned in turn from the left and top until the brightness of the scanned image is larger than a specified threshold. The scanning of (c-2)–(c-4) are similar to the scanning of (c-1). The positions of the detected data are recorded as $\boldsymbol{\xi}_i := (u_i, v_i) \in \mathbb{R}^2$ $(i = 1, \cdots, 4)$. Consider the

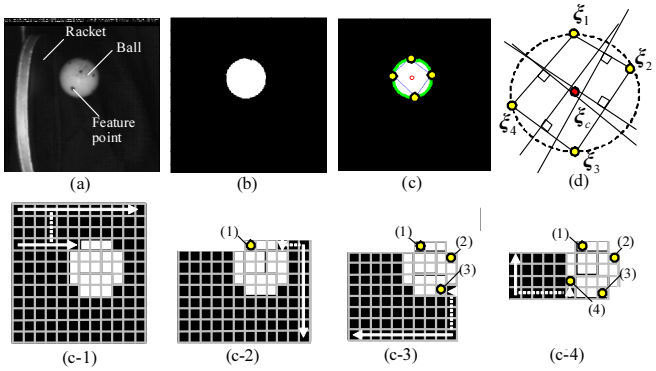

Fig. 3. Image data and detection of the center of the ball.

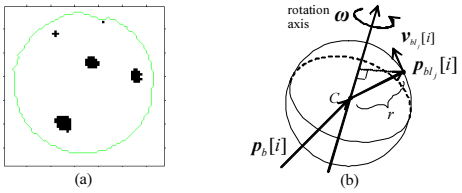

Fig. 4. Image data and calculation of the rotational velocity.

mediators of the lines between $\boldsymbol{\xi}_{i+1}$ and $\boldsymbol{\xi}_i$ $(i = 1, \cdots, 4)$, $\boldsymbol{\xi}_5 := \boldsymbol{\xi}_1$ as shown in Fig. 3 (d). Define $\boldsymbol{\xi}_c$ as the center of the ball. The center $\boldsymbol{\xi}_c$ is obtained by the least squares method with the performance function, which is the sum of the squares of the distances of $\boldsymbol{\xi}$ from the mediators. The center of the ball $\boldsymbol{p}_b$ is calculated by $\boldsymbol{\xi}_c$ in the left and right images [8]. The translational velocities of the ball by the mean of all the velocities between the $(i+1)$th and ith position as

$$\boldsymbol{v}_b = \frac{\sum_{i=0}^{N-2} \boldsymbol{v}_b[i]}{N-1}, \ \boldsymbol{v}_b[i] := \frac{\boldsymbol{p}_b[i+1] - \boldsymbol{p}_b[i]}{\Delta t}, \quad (1)$$

where $\Delta t = 1/900$ [s] is the sampling time and N is the number of the frames. Note that $[i]$ denotes the ith frame.

Next, consider the detection of the rotational velocity of the ball. Figure 4 (a) shows the feature points which are marked on the ball as the black prints. This image can be obtained by the appropriate gray scale transformation, sharpening and binarization. Figure 4 (b) shows the ball in the ith frame, where $\boldsymbol{\omega} \in \mathbb{R}^3$ is the rotation axis, $\boldsymbol{p}_{bl_j} := \boldsymbol{p}_{l_j} - \boldsymbol{p}_b$ and $\boldsymbol{p}_{l_j} \in \mathbb{R}^3$ is the feature point on the ball $(j = 1, \cdots, N_l)$. For the $j$the feature point, the following rotational relationship holds [9]:

$$\boldsymbol{p}_{bl_j}[i+1] = e^{\widehat{\omega}\Delta t} \boldsymbol{p}_{bl_j}[i], \ e^{\widehat{\omega}\Delta t} \approx \boldsymbol{I}_3 + \widehat{\boldsymbol{\omega}}\Delta t, \quad (2)$$

where $\widehat{\boldsymbol{\omega}} \in \mathbb{R}^{3\times3}$ is the skew-symmetric matrix which corresponds to the cross product of $\boldsymbol{\omega}$. Note that the terms of the higher order with respect to Δt are approximated to 0 because of the small Δt. Substituting the 2nd eq. into the 1st eq. of (2) leads to

$$\boldsymbol{p}_{bl_j}[i+1] = \boldsymbol{p}_{bl_j}[i] + \Delta t \widehat{\boldsymbol{\omega}} \boldsymbol{p}_{bl_j}[i],$$

where $\widehat{\boldsymbol{\omega}} \boldsymbol{p}_{bl_j}[i]$ is calculated as

$$\widehat{\boldsymbol{\omega}} \boldsymbol{p}_{bl_j}[i] = \boldsymbol{\omega} \times \boldsymbol{p}_{bl_j}[i] = -\boldsymbol{p}_{bl_j}[i] \times \boldsymbol{\omega} = -\widehat{\boldsymbol{p}}_{bl_j}[i] \times \boldsymbol{\omega}.$$

Then, we get

$$\widehat{\boldsymbol{p}}_{bl_j}[i]\boldsymbol{\omega} = -\boldsymbol{v}_{bl_j}[i], \boldsymbol{v}_{bl_j}[i] := \frac{\boldsymbol{p}_{bl_j}[i+1] - \boldsymbol{p}_{bl_j}[i]}{\Delta t}. \quad (3)$$

III. Modeling of Rebound

A. Rebound between the ball and table

Figure 5 shows the rebound of the ball from the table, where $(\boldsymbol{v}_b, \boldsymbol{\omega}_b)$ and $(\boldsymbol{v}_b', \boldsymbol{\omega}_b')$ are the translational and rotational velocities of the ball just before and after the rebound and Σ_B is the reference frame with the z-axis normal to the table. The simplest model of the rebound phenomenon is described by the equations of $v_{bz}' = -e_t v_{bz}$, $v_{bx}' = v_{bx}$

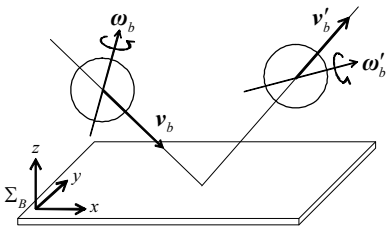

Fig. 5. Ball velocities just before and after the rebound.

and $v'_{by} = v_{by}$, where e_t is the coefficient of restitution of the table in the z direction. In this model, it is assumed that there is no friction on the table. Therefore, the components x and y of the velocity $\boldsymbol{v}_b$ do not change. However, since there actually *exists the friction*, the velocity $\boldsymbol{v}'_b$ just after the rebound changes due to the friction and the rotational velocity $\boldsymbol{\omega}_b$ as shown in Fig. 6. The red and blue circles represent the cases of the top and back spins respectively and the ball velocities just before the rebound are the same. It is easily confirmed that the velocity v'_{bz} in the case of the back spin is greater than in the case of the top spin. In addition, the rotational velocity $\boldsymbol{\omega}'_b$ also changes due to the friction. In order to predict the ball trajectory after the rebound from the table, it is necessary to consider the friction.

For integrating the effect of the friction in the rebound model, it is very important to consider the *type of the contact* during the impact, i.e., the sliding and rolling contact. This can be determined by using the tangent velocity given by

$$\boldsymbol{v}_{bT} := [v_{bx}\ v_{by}\ 0]^{\mathrm{T}} + \boldsymbol{\omega} \times \boldsymbol{r} = \begin{bmatrix} v_{bx} - r\omega_{by} \\ v_{by} + r\omega_{bx} \\ 0 \end{bmatrix}, \quad (4)$$

where $\boldsymbol{r} := [0\ 0\ -r]^{\mathrm{T}} \in \mathbb{R}^3$ is the contact point of the ball from its center and $r \in \mathbb{R}_+$ is the ball radius. For the modeling, we make the following assumptions:

Assumption 1: During the impact of the rebound, the type of the contact between the ball and table is a point contact. This means that any moment does not effect on the ball during the impact.

Assumption 2: The differences between the translational and angular momentums before and after the rebound equal the impulses at the rebound. Therefore, the impulse of the rotation is given by $\boldsymbol{r} \times \boldsymbol{P}$, where $\boldsymbol{P} \in \mathbb{R}^3$ is the impulse in the translational direction.

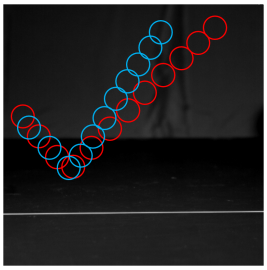

Fig. 6. Deference of $\boldsymbol{v}'_b$ when $\boldsymbol{\omega}_b$ is the top or back spin.

Assumption 3: The following simple bounce relationship in the z direction holds:

$$v'_{bz} = -e_t v_{bz} \quad (5)$$

Assumption 4: The impulse in the x and y directions $\boldsymbol{P}_{xy} := [P_x\ P_y\ 0]^{\mathrm{T}} \in \mathbb{R}^3$ is given by

$$\boldsymbol{P}_{xy} = -\lambda \frac{\boldsymbol{v}_{bT}}{\|\boldsymbol{v}_{bT}\|},\ 0 \le \lambda \le \mu |P_z|, \quad (6)$$

where μ is the dynamical coefficient of friction between the ball and table.

Assumption 5: The contact velocities $\boldsymbol{v}_b$ and $\boldsymbol{v}'_b$ just before and after the rebound are in the same direction. That is, the following relation holds:

$$\boldsymbol{v}'_{bT} = \nu \boldsymbol{v}_{bT},\ \nu \ge 0. \quad (7)$$

If $\nu \neq 0$, $\lambda = \mu |P_z|$.

Assumptions 4 and 5 are necessary to express the sliding and rolling contacts during the impact. Assumption 4 means that the impulse in the x and y directions is related to the one in the z direction as shown in Fig. 7 (a), where the friction force in the x and y directions is proportional to f_z with μ and its direction is the opposite of $\boldsymbol{v}_{bT}$. λ in (6) is the magnitude of $\boldsymbol{P}_{xy}$ and is equal to or smaller than $\mu |P_z|$ because the contact can be changed from sliding to rolling during the impact as shown in Fig. 7 (b). Note that the static friction force does not work on the ball when the contact is rolling. Assumption 5 means that the tangent velocity $\boldsymbol{v}'_{bT}$ after the rebound does not become negative because the rolling starts just after $\boldsymbol{v}'_{bT} = \boldsymbol{0}$. The condition of $\nu \neq 0$ means that the contact is sliding during the impact.

From Assumptions 1, 2, the following equations hold:

$$m\boldsymbol{v}'_b - m\boldsymbol{v}_b = \boldsymbol{P} \quad (8)$$

$$I\boldsymbol{\omega}'_b - I\boldsymbol{\omega}_b = \boldsymbol{r} \times \boldsymbol{P}, \quad (9)$$

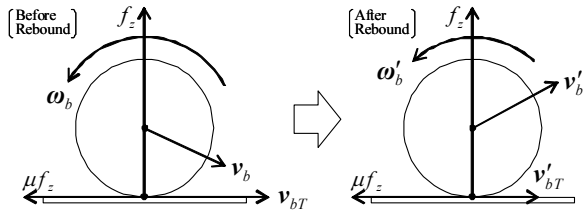

(a) Case where the contact is sliding during the impact

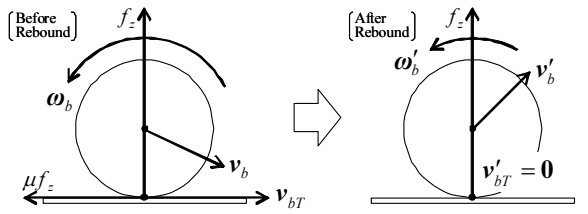

(b) Case where the contact is changed from sliding to rolling during the impact

Fig. 7. Sliding and rolling during the impact.

where m and $I = \frac{2}{3}mr^2$ are the mass and moment of inertia. Combining (5) and (8) yields the relation in the z direction:

$$P_z = -m(1+e_t)v_{bz}. \tag{10}$$

For deriving the relation in the x and y directions, the tangent velocity $\boldsymbol{v}_b'$ after the rebound is calculated by the definition of (4) with (8), (9) and Assumption 4:

$$\boldsymbol{v}_{bT}' = -\lambda\left(\frac{1}{m}+\frac{r^2}{I}\right)\frac{\boldsymbol{v}_{bT}}{\|\boldsymbol{v}_{bT}\|}+\boldsymbol{v}_{bT}. \tag{11}$$

The tangent velocity after the rebound, $\boldsymbol{v}_{bT}'$, has to satisfy (7) of Assumption 5. Substituting (11) into (7) yields

$$\nu = -\frac{\lambda}{\|\boldsymbol{v}_{bT}\|}\left(\frac{1}{m}+\frac{r^2}{I}\right)+1. \tag{12}$$

It is sufficient to check whether ν of (12) is positive or not when the contact during the impact is supposed to be sliding, that is, $\lambda = \mu|P_z|$. Combining $\lambda = \mu|P_z|$, (10), $I = \frac{2}{3}mr^2$ and (12) leads to

$$\nu_s := 1 - \frac{5}{2}\mu(1+e_t)\frac{|v_{bz}|}{\|\boldsymbol{v}_{bT}\|}, \tag{13}$$

which is defined as ν in the case of the sliding. It follows that (i) if $\nu_s > 0$, $\nu = \nu_s$ and $\lambda = \mu|P_z|$ (the case of the sliding); (ii) if $\nu_s \leq 0$, $\nu = 0$ (the case of the rolling).

Let us consider the sliding case of (i). Substituting (6) with $\lambda = \mu|P_z|$ and (10) into (8) and (9), we get the translational and rotational velocities after the rebound, $\boldsymbol{v}_b'$ and $\boldsymbol{\omega}_b'$, as the functions of those before the rebound:

$$\boldsymbol{v}_b' = \boldsymbol{A}_v\boldsymbol{v}_b + \boldsymbol{B}_v\boldsymbol{\omega}_b \tag{14}$$

$$\boldsymbol{\omega}_b' = \boldsymbol{A}_\omega\boldsymbol{v}_b + \boldsymbol{B}_\omega\boldsymbol{\omega}_b, \tag{15}$$

where

$$\boldsymbol{A}_v := \begin{bmatrix} 1-\alpha & 0 & 0 \\ 0 & 1-\alpha & 0 \\ 0 & 0 & -e_t \end{bmatrix}, \boldsymbol{B}_v := \begin{bmatrix} 0 & \alpha r & 0 \\ -\alpha r & 0 & 0 \\ 0 & 0 & 0 \end{bmatrix}$$

$$\boldsymbol{A}_\omega := \begin{bmatrix} 0 & -\frac{3\alpha}{2r} & 0 \\ \frac{3\alpha}{2r} & 0 & 0 \\ 0 & 0 & 0 \end{bmatrix}, \boldsymbol{B}_\omega := \begin{bmatrix} 1-\frac{3\alpha}{2} & 0 & 0 \\ 0 & 1-\frac{3\alpha}{2} & 0 \\ 0 & 0 & 1 \end{bmatrix}$$

$$\alpha := \mu(1+e_t)\frac{|v_{bz}|}{\|\boldsymbol{v}_{bT}\|}. \tag{16}$$

Next consider the rolling case of (ii). From $\nu = 0$ and (12), λ is given by

$$\lambda = \frac{2}{5}m\|\boldsymbol{v}_{bT}\|. \tag{17}$$

By the similar calculation of the case (i) with (17), we get the coefficient matrices of (14) and (15) as follows:

$$\boldsymbol{A}_v := \begin{bmatrix} \frac{3}{5} & 0 & 0 \\ 0 & \frac{3}{5} & 0 \\ 0 & 0 & -e_t \end{bmatrix}, \boldsymbol{B}_v := \begin{bmatrix} 0 & \frac{2r}{5} & 0 \\ -\frac{2r}{5} & 0 & 0 \\ 0 & 0 & 0 \end{bmatrix}$$

$$\boldsymbol{A}_\omega := \begin{bmatrix} 0 & -\frac{3}{5r} & 0 \\ \frac{3}{5r} & 0 & 0 \\ 0 & 0 & 0 \end{bmatrix}, \boldsymbol{B}_\omega := \begin{bmatrix} \frac{2}{5} & 0 & 0 \\ 0 & \frac{2}{5} & 0 \\ 0 & 0 & 1 \end{bmatrix}. \tag{18}$$

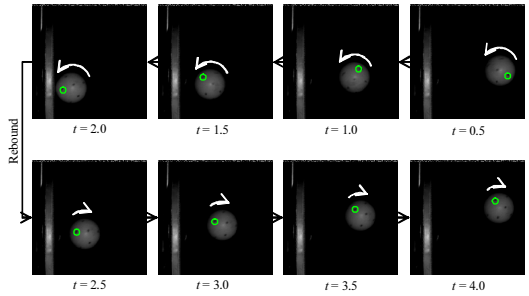

Fig. 8. Rebound of the ball from the racket rubber.

B. Rebound between the ball and racket rubber

Figure 8 shows an example of the rebound of the ball from the racket rubber. The green circles represent the same point on the ball. It is confirmed that the rotational velocity about the axis normal to the image plane changes to the *inverse* direction after the rebound. This implies that the contact velocities between the ball and the rubber before and after the rebound are opposite to each other. This can not be expressed by considering only the friction and is the specific phenomenon in the case of the rubber due to the storage of its elastic energy. In order to achieve desired ball trajectory after the rebound from the racket, it is necessary to consider this phenomenon.

Figure 9 (a) shows the rebound of the ball from the racket rubber, where the meanings of the variables are the same as in Section 3.1 with respect to the racket frame Σ_R attached to the racket as the z-axis normal to the surface. In order to express the effect of the elasticity parallel to the surface, we model the tangent motion of the racket rubber as the motion of the virtual mass m_α with the spring k_s and the distance $\boldsymbol{s}(t) \in \mathbb{R}^3$ as shown in Fig. 9 (b). Note that m_α is the equivalent mass consisting of the mass of the ball and the deformed area of the rubber.

For the model, we make the following assumptions:

Assumption 6: The rebound in the z direction does not cause any effect in the x and y directions.

Assumption 7: The impulse in the x and y directions $\boldsymbol{P}_{xy} \in \mathbb{R}^3$ is related to the tangent velocity $\boldsymbol{v}_{bT}$ by

$$\boldsymbol{P}_{xy} = -k_p\boldsymbol{v}_{bT}. \tag{19}$$

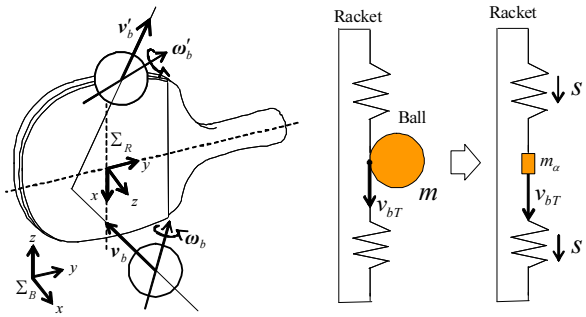

(a) Rebound between the ball and the rubber (b) Virtual spring model parallel to the surface

Fig. 9. The rebound between the ball and the rubber.

Assumptions 1–4 are also assumed to hold here. From Assumption 1–3 and 6, the equations of (8), (9) and (10) also hold here. Combining (19), (8), (9) and (10), we get the translational and rotational velocities after the rebound, $(\boldsymbol{v}_b', \boldsymbol{\omega}_b')$, are given by the same functional relationships as (14) and (15) with the coefficient matrices as follows:

$$\boldsymbol{A}_v := \begin{bmatrix} 1-k_{pv} & 0 & 0 \\ 0 & 1-k_{pv} & 0 \\ 0 & 0 & -e_r \end{bmatrix}, \boldsymbol{B}_v := k_{pv} \begin{bmatrix} 0 & r & 0 \\ -r & 0 & 0 \\ 0 & 0 & 0 \end{bmatrix}$$
$$\boldsymbol{A}_\omega := k_{p\omega} \begin{bmatrix} 0 & -r & 0 \\ r & 0 & 0 \\ 0 & 0 & 0 \end{bmatrix}, \boldsymbol{B}_\omega := \begin{bmatrix} 1-k_{p\omega}r^2 & 0 & 0 \\ 0 & 1-k_{p\omega}r^2 & 0 \\ 0 & 0 & 1 \end{bmatrix}$$
$$k_{pv} := \frac{k_p}{m}, \ k_{p\omega} := \frac{k_p}{I}, \tag{20}$$

where e_r is the coefficient of restitution of the rubber.

IV. Model Verification

The parameters of the ball are $m = 2.7 \times 10^{-3}$[kg] and $r = 2.0 \times 10^{-2}$[m]. The coefficient of restitution of the table e_t can be calculated as

$$e_t = \sqrt{\frac{h_2}{h_1}}, \tag{21}$$

where h_1 and h_2 are the first and second heights of the dropped ball. e_t is identified as $e_t = 0.93$ by averaging 25 data points. The dynamical friction coefficient μ is estimated as $\mu = 0.25$ by measuring the drastic change in the value of the spring balance instrument at the sliding where the weighted ball on the table with the weight 2.0[kg] was pulled.

A. The case of the rebound on the table

The rebound model on the table is verified by the 4 cases of (a) Top spin, (b) Back spin, (c) Side-top spin and (d) Side-back spin as illustrated in Fig. 10. Figure 11 shows the verifications of the cases of the top and back spins, where the circles and squares represent the top and back spins. Since the experimental data of (a) and (b) is the cases of the pure top spin ($\omega_{by} < 0$) and pure back spin ($\omega_{by} > 0$) with $v_{by}, \ \omega_{bx}, \ \omega_{bz} \simeq 0$, (v_{bx}, v_{bz}) [m/s] and

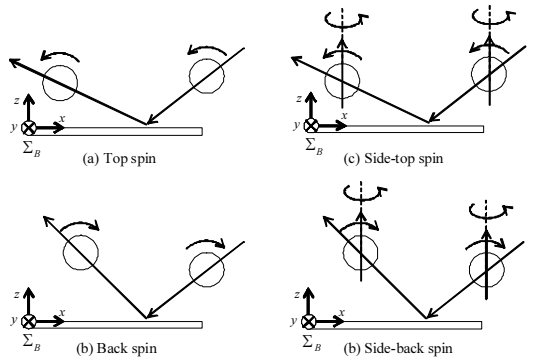

Fig. 10. Situations of the verification of the table.

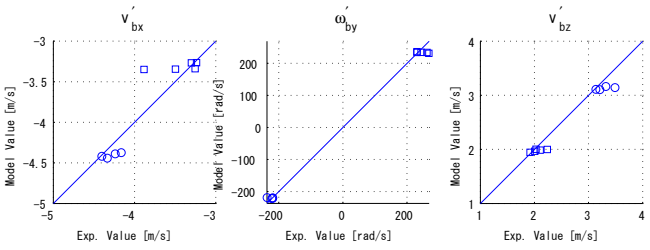

Fig. 11. Verification of the top and side spins.

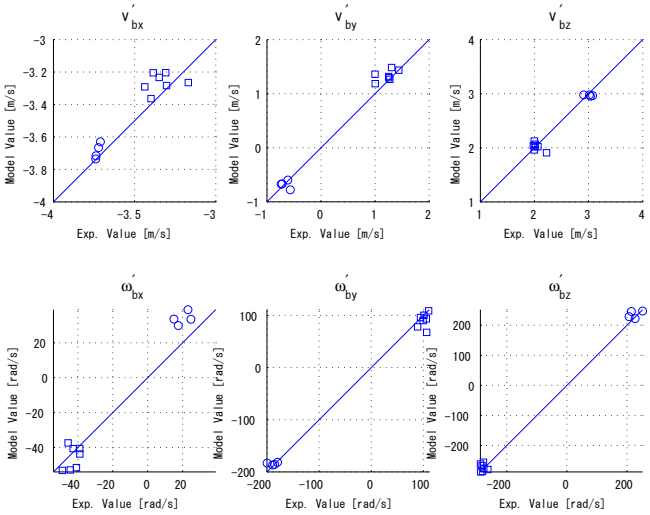

Fig. 12. Verification of the side-top and side-back spins.

ω_{by} [rad/s] are only shown. The horizontal and vertical axes are the experimental values and the calculated values from the model of the translational and rotational velocities after the rebound. The solid lines represent the cases where these values are the same. The general situations are represented by Fig. 12, which shows the cases with the multi rotational axes where the circles and squares represent the side-top and side-back spins. Note that the side spin is $\omega_{bz} > 0$, the top spin is $\omega_{by} < 0$ and the back spin is $\omega_{by} > 0$. It is confirmed that the almost data in Figs. 11 and 12 are close to the solid lines. It may be caused by the quantization errors of the image data that a few data is a little far from the solid lines. The image coordinates (u, v) is related to the cartesian ones (x_c, y_c, z_c) as $u = \frac{f}{\alpha_u}\frac{x_c}{z_c}$ and $v = \frac{f}{\alpha_v}\frac{y_c}{z_c}$, where the parameters f, (α_u, α_v) are shown in Section 2. $z_c = 1.2$[m] is in the optic axis and the distance between the ball and the camera. The bigger errors of the translational and rotational velocities are about 0.5[m/s] and 20[rad/s]. The corresponding distances in (x_c, y_c) of the errors in a frame are calculated as $e^v_{xy} = 0.5 \times \Delta t$ and $e^\omega_{xy} = r \times 20 \times \Delta t$. From the relationships $u = \frac{f}{\alpha_u}\frac{x_c}{z_c}$ and $v = \frac{f}{\alpha_v}\frac{y_c}{z_c}$, the errors in (u, v) are calculated as $e^v_{uv} = 0.81$ and $e^\omega_{uv} = 0.64$ [pixel]. Since e^v_{uv} and e^ω_{uv} are smaller than 1 [pixel], the errors of 0.5 [m/s] and 20 [rad/s] may be caused by the quantization errors. Because all the errors in Figs. 11 and 12 are smaller than these errors, the experimental data shows the validation

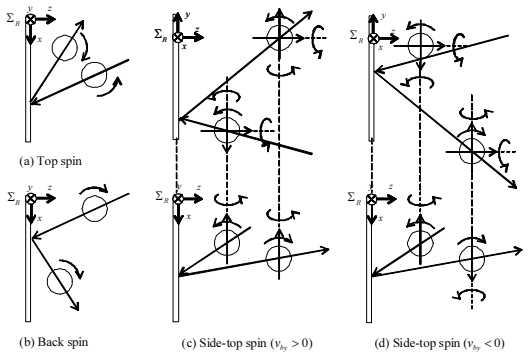

Fig. 13. Situations of the verification of the racket.

of the rebound model on the table.

B. The case of the rebound on the racket

The rebound model on the racket is verified by the 4 cases of (a) Top spin, (b) Back spin, (c) Side-top spin ($v_{by} > 0$) and (d) Side-back spin ($v_{by} < 0$) as illustrated in Fig. 13. The parameters in the rebound model are indentified as $e_r = 0.81$, $k_p = 1.9 \times 10^{-3}$ [1/kg]. Figures 14 and 15 show the case of the pure top and back spins and the case of the side-top spin of $v_{by} > 0$ and $v_{by} < 0$. The red data is used for the identification of the parameters and the blue data is used for the verification. The circles and squares represent the top and back spin in Fig. 14 and the side-top spin of $v_{by} > 0$ and the one of $v_{by} < 0$ in Fig. 15. It is confirmed that the red and blue data are close to the solid lines with the errors due to the quantization errors of the image data.

Table I shows some of the experimental data of the contact velocities before and after the rebound and the ones after the rebound which are calculated by the model. It is confirmed that the calculated velocities are in the opposite directions of the velocities before the rebound and close to the velocities after the rebound. Therefore, the proposed model can represent the specified effect of the rubber.

V. Conclusions

We derived analytical models of the rebound phenomenon between a ping-pong ball and the table/racket rubber. In the rebound model of the table, the determination of the type of the contact during the impact was derived as a generalized condition in the 3-dimensional space. In the model between the ball and racket rubber, it was assumed

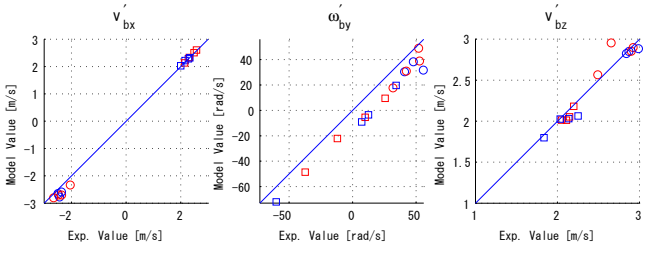

Fig. 14. Verification of the top spin and back spin.

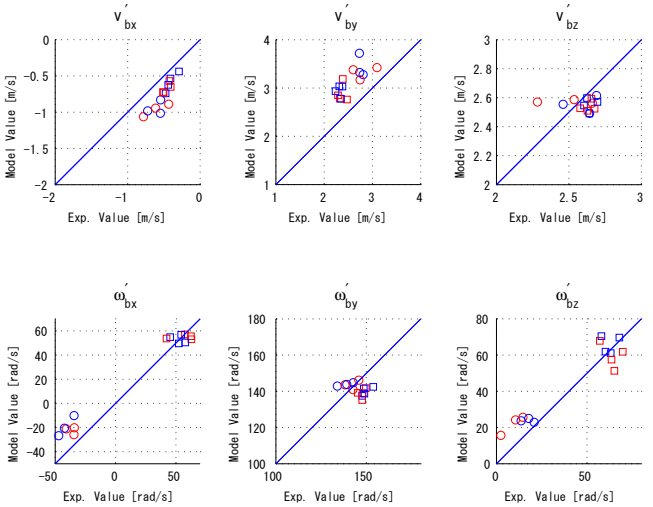

Fig. 15. Verification of the side-top spins of $v_{by} > 0$ and $v_{by} < 0$.

TABLE I
VERIFICATION OF THE TANGENT VELOCITY

No.	Before the rebound	After the rebound	Calculated by Model
1	−3.79	2.35	2.21
2	−3.87	2.12	2.26
3	−3.77	2.04	2.20
4	−3.92	2.03	2.29
5	−3.68	2.02	2.15
6	−3.74	2.37	2.18

that the kinetic energy of the tangent velocity was stored as the potential energy due to the elasticity of the rubber. This assumption led to that the impulse in the horizontal direction is proportional to the tangent velocity. The models were verified by experimental data.

As future work, it is necessary to reduce the quantization errors and verify the model in additional rebound situations. Furthermore, we would try to make a method to detect the ball state in real-time.

References

[1] R. Garwin, “Kinematics of an ultraelastic rough ball,” *Am. J. Phys.*, Vol.37, pp.88–92 1969.
[2] H. Brody, “That’s how the ball bounces,” *Phys. Teach.*, Vol.22 pp.494–497, 1984.
[3] Kanji Shibukawa, *Dynamics of Physical Exercise*, Daishukanshoten, 1969 (in japanease).
[4] R. Cross, “Effects of friction between the ball and strings in tennis,” *Sports Eng.*, Vol.3, pp.85–97, 2000.
[5] R. Cross, “Measurements of the horizontal coefficient of restitution for a superball and a tennis ball,” *Am. J. Phys.*, Vol.70, No.5, pp.482–489, 2001.
[6] R. Cross, “Bounce of a spinning ball near normal incidence,” *Am. J. Phys.*, Vol.73, No.10, pp.914–920, 2005.
[7] R. Cross, “The bounce of a ball,” *Am. J. Phys.*, Vol.67, No.3, pp.222–227, 1999.
[8] B. K. Ghosh, N. Xi and T. J. Tarn, *Control in Robotics and Automation: Sensor-Based Integration*, Academic Press, 1999.
[9] R. M. Murray, Z. Li and S. S. Sastry, *A Mathematical Introduction to ROBOTIC MANIPULATION*, CRC Press, 1994.